Ceramics International 42 (2016) 10913–10921

Contents lists available at ScienceDirect

Ceramics International

journal homepage: www.elsevier.com/locate/ceramint

Synthesis and morphological transformation of $BaWO_4$ crystals: Experimental and theoretical insights

Marisa Carvalho Oliveira [a,b], Lourdes Gracia [a], Içamira Costa Nogueira [c], Maria Fernanda do Carmo Gurgel [d], Jose Manuel Rivas Mercury [c], Elson Longo [e], Juan Andrés [a,*]

[a] Department of Analytical and Physical Chemistry, University Jaume I (UJI), Castelló E-12071, Spain
[b] CDMF-UFSCar, Universidade Federal de São Carlos, PO Box 676, 13565-905 São Carlos, SP, Brazil
[c] PPGEM-IFMA, Instituto Federal do Maranhão, CEP 65030-005 São Luís, MA, Brazil
[d] Department of Chemistry, Universidade Federal de Goiás, Regional Catalão, Av.Dr.Lamartine Pinto de Avelar, 75704-020 Catalão, GO, Brazil
[e] CDMF-UNESP, Universidade Estadual Paulista, PO Box 355, CEP 14801-907 Araraquara, SP, Brazil

ARTICLE INFO

Article history:
Received 16 February 2016
Received in revised form
18 March 2016
Accepted 29 March 2016
Available online 30 March 2016

Keywords:
$BaWO_4$ crystals
Co-precipitation method
Morphology
DFT calculations
Surface energies

ABSTRACT

$BaWO_4$ crystals have been obtained by a co-precipitation method, and their structures were characterized by X-ray diffraction and Rietveld refinement techniques, while field emission scanning electron microscopy was utilized to investigate the morphology of the as-synthesized aggregates. Geometries, bulk electronic properties, surface energies, and surface tension of the obtained $BaWO_4$ crystals were evaluated using first-principles quantum mechanical calculations. A theoretical model based on the Wulff construction was introduced to explain possible crystal morphologies by tuning their surface chemistry, which is related to the relative stability of the faceted crystals. Both the experimental and theoretical data revealed the presence of (112), (001), and (100) facets with low values of surface energy in the $BaWO_4$ crystals. The experimental morphologies of the as-synthesized samples are similar to the theoretically obtained shapes when surface energy values for the (001) and (100) surfaces are increased simultaneously.

1. Introduction

Barium tungstate ($BaWO_4$) crystals have attracted significant interest from many research groups due to their potential applications in scintillation devices, batteries, capacitors, photocatalysts, and, in particular, photoluminescent materials [1–6]. In recent years, various synthetic methods have been used to produce $BaWO_4$ crystals, such as co-precipitation (CP), sol–gel, modified Pechini, solid state reaction, solution route, Czochralski, sonochemical, and hydrothermal techniques [7–24].

$BaWO_4$ is a semiconductor that belongs to the family of scheelites with crystallized tetragonal structures having the space group $I4_1/a$ and symmetry C_{4h}^6, in which Ba atoms are coordinated to eight O atoms, while W atoms have tetragonal coordination of O atoms; thus, the building blocks of the $BaWO_4$ crystal are deltahedral [BaO_8] and tetrahedral [WO_4] clusters [14,25–30]. Distortions of these clusters caused by the deformations of W–O and Ba–O bond distances as well as by tilting of O–W–O and O–Ba–O bond angles have a significant effect on their geometry, surface structure, and related properties [14]. Various theoretical studies have been published on the geometry as well as electronic and optical properties of $BaWO_4$ [19,31–33].

Surface properties of materials strongly depend on their morphology that is characterized by types and relative areas of various crystal facets, which usually can be tuned by tailoring their facets with different surface atomic arrangements and coordination. In general, the most stable surfaces control the crystal growth process, while less stable crystal facets contain large numbers of kink atoms in high-index planes [34]. Thus, studying the morphology of micro- and nanomaterials is an essential step in understanding their physical and chemical properties, while controlled synthesis of specific morphologies is critical for enhancing their performance in practical applications [35,36]. In particular, morphology-controlled syntheses of $BaWO_4$ have been performed by various research groups [37–40]. Nevertheless, these methods are far from being optimized, and their experimental aspects are still debated. In this context, experimental surface energies cannot be readily attained, and computer modeling and simulations are necessary to obtain surface characteristics of $BaWO_4$, which are powerful tools for exploring morphological mechanisms at the atomistic/molecular level.

* Corresponding author.
E-mail address: andres@uji.es (J. Andrés).

http://dx.doi.org/10.1016/j.ceramint.2016.03.225
0272-8842/

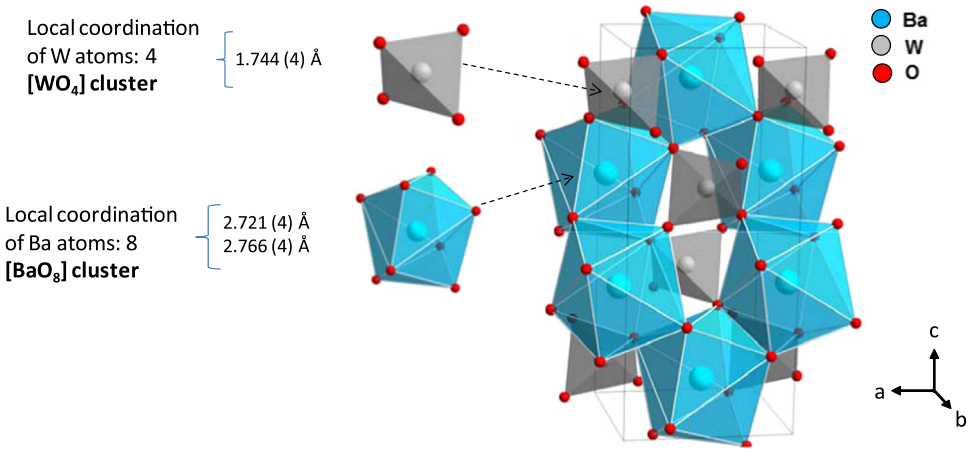

Fig. 1. A polyhedral representation of the $BaWO_4$ unit cell. The local coordination corresponding to the deltahedral [BaO_8] and tetrahedral [WO_4] clusters is depicted for both Ba and W atoms, respectively.

Using a specific methodology, which has been applied to study morphologies of various metal oxides such as SnO_2 [41], $PbMoO_4$ [42], and $CaWO_4$ [43], we developed a combination of experimental studies with first-principles calculations to deeper investigate electronic, structural, and energetic properties controlling the morphology and related transformation mechanisms of various metals and metal oxides such as Ag, anatase TiO_2, $BaZrO_3$, and α-Ag_2WO_4 [44] as well as Co_3O_4, Fe_2O_3, and In_2O_3 [45]. Based on the obtained results, we were able to explore facet-dependent photocatalytic and antibacterial properties of α-Ag_2WO_4 crystals [46] as well as the relationship between the photoluminescence and photocatalytic properties of Ag_3PO_4 microcrystals [47] and then identify and rationalize morphological, structural, and optical properties of β-Ag_2MoO_4 microcrystals [48]. These cited papers contain a description of the method of calculating surface energies, which were used to characterize the corresponding surface morphologies.

The main goal of this article is to investigate the morphology of the as-synthesized $BaWO_4$ crystals characterized by X-ray diffraction and Rietveld refinement and field emission scanning electron microscopy techniques, as well as to simulate the crystal shape possibilities using first-principles quantum mechanical calculations based on the Wulff construction.

2. Experimental

2.1. Synthesis of $BaWO_4$ crystals

$BaWO_4$ crystals were synthesized by a CP method at 353 K in aqueous solutions. A typical synthesis procedure for the $BaWO_4$ crystals can be described as follows: 1×10^{-3} mol of sodium tungstate dihydrate ($Na_2WO_4 \cdot 2H_2O$) (99.5% purity, Stream Chemical) and 1×10^{-3} mol of barium nitrate [$Ba(NO_3)_2$] (99% purity, Sigma-Aldrich) salts were dissolved in two separate beakers containing 50 mL of deionized water under constant stirring until it reaches 353 K. Next, the barium nitrate solution was added to the sodium tungstate dihydrate solution and maintained under agitation at 353 K for 20 min. As a result, a white precipitate was rapidly formed, which was washed with deionized water several times. Finally, the obtained white precipitates were collected and dried in a conventional furnace at 323 K for 8 h.

2.2. Characterization

$BaWO_4$ crystals were structurally characterized by X-ray diffraction (XRD) using a DMax/2500PC diffractometer (Rigaku, Japan) with Cu Kα radiation ($\lambda = 1.5406$ Å) in a 2θ range from 10° to 110° with an angular step of 0.02° min^{-1}. Rietveld refinement [49] of the obtained XRD patterns was performed by using a general structure analysis (GSAS) program [50]. The diffraction peak profiles were adjusted by utilizing Thompson-Cox-Hastings pseudo-Voigt (pV-TCH) and asymmetry functions as described by Finger et al. [51] Strain anisotropy broadening was corrected by applying a phenomenological model described by Stephens [52]. Morphologies of the synthesized $BaWO_4$ crystals were studied with a field-emission scanning electron microscope (FE–SEM) (model Inspect F50, FEI Company, Hillsboro, OR) operated at 15 kV.

2.3. Computational methods and modeling

First-principles calculations were conducted within the framework of the density functional theory (DFT) using the CRYSTAL14 software package [53]. The gradient-corrected correlation functional by Lee et al. [54] combined with the Becke's exchange functional (B3LYP) [55] was used for all calculations. This method has been successfully employed in various studies of bulk and surface electronic and structural properties of perovskite [56,57], tungstate [42,58,59], and molybdate-based materials [60]. Diagonalization of the Fock matrix was performed at adequate k-points grids (Pack–Monkhorst 1976) in the reciprocal space. The thresholds controlling the accuracy of the Coulomb and exchange integral calculations were set to 10^{-8} (ITOL1 to ITOL4) and 10^{-14} (ITOL5), respectively, whereas the percentage of Fock/Kohn–Sham matrices mixing was set to 30 (IPMIX = 30) [61]. The W atoms were described by large-core effective core potentials derived by Hay and Wadt and modified by Cora et al. [62], while the O [63] and Ba [64] atoms were represented by the 6-31G* basis set.

The surface energy, E_{surf} [43,45], was calculated by using the equation $(E_{slab} - nE_{bulk})/½A$, where nE_{bulk} is the number of surface molecular units multiplied by the energy of the bulk, E_{slab} is the total energy of the surface slab per molecular unit, and A is the surface area. The equilibrium shape of a crystal can be calculated by utilizing Wulff constructions that minimize the total surface free energy at a fixed volume, providing a simple relationship between the surface energy, E_{surf}, of a (hkl) plane and its distance from the center of the crystallite in the normal direction [65]. The Visualization for Electronic and Structural Analysis (VESTA) program [66] has been utilized to obtain morphologies of the $BaWO_4$ crystals. Band structures were calculated for 80 k-points along the appropriate high-symmetry paths of the adequate Brillouin zone.

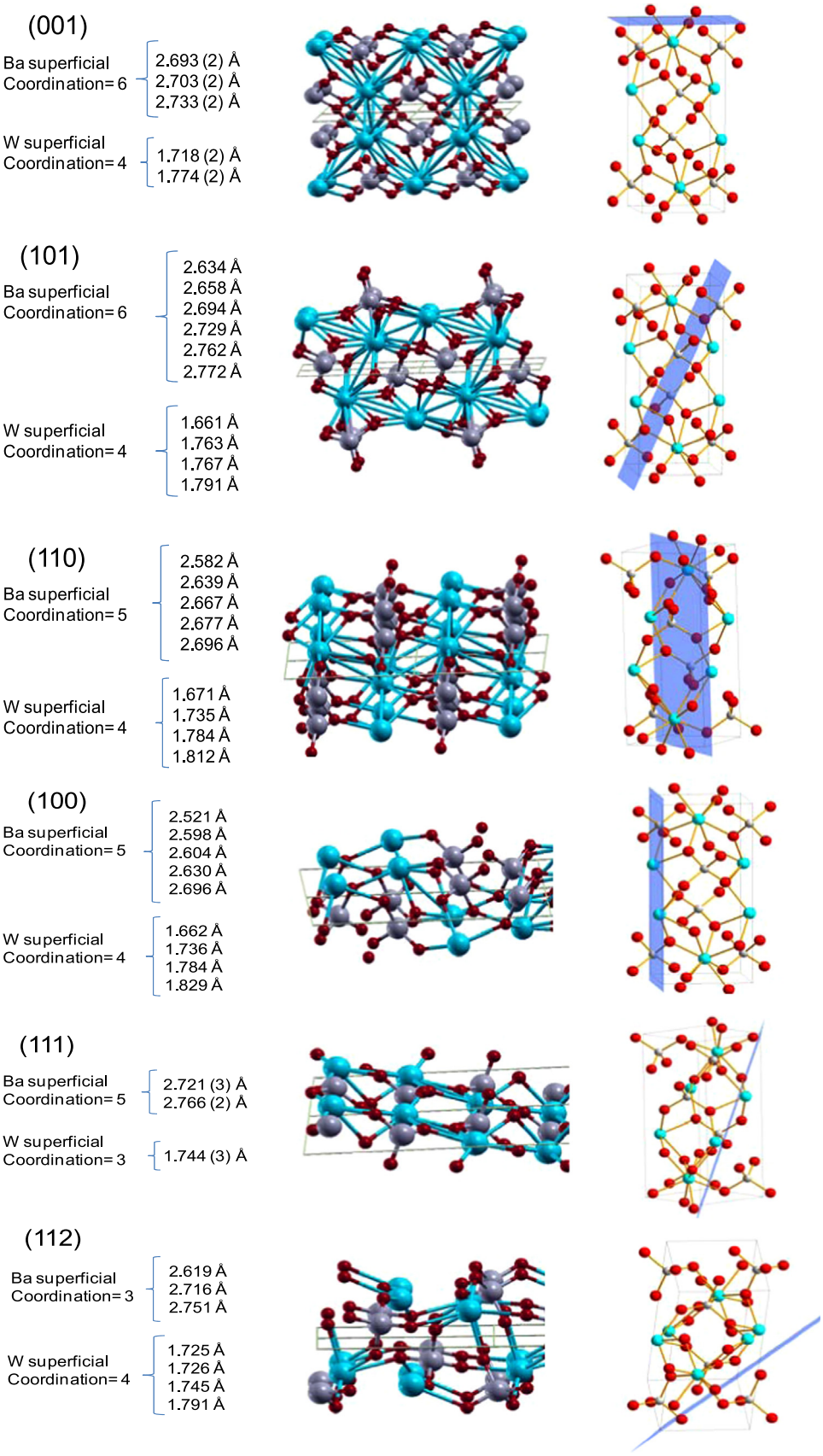

Fig. 2. Schematic representations of the (001), (101), (110), (100), (111), and (112) surfaces. The values of Ba–O and W–O bond distances are listed for the superficial Ba and W atoms, respectively.

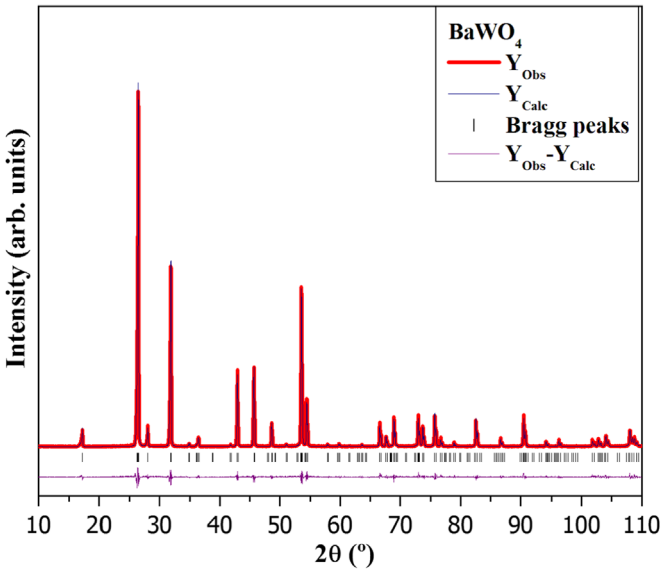

Fig. 3. Rietveld refinements for the $BaWO_4$ crystals.

Table 1
Calculated and experimental values of the lattice parameters (a and c) and atomic coordinates of the O_x, O_y, and O_z.

Data	Cell parameters		Oxygen coordinates		
	a (Å)	c (Å)	O_x	O_y	O_z
Theo. (this work)	5.5927	12.4055	0.2245	0.1219	0.04635
Exp. (this work)	5.6149	12.7326	0.2295	0.1294	0.05024
Exp. [5]	5.6102	12.7100	–	–	–
Exp. [2]	5.6063	12.7107	0.76731	0.14013	0.08188
Exp. [6]	5.615 (2)	12.722 (4)	0.2422 (2)	0.1403 (3)	0.0369 (9)
Exp. [10]	5.612	1 2.706	–	–	–
Exp. [14]	5.5682	12.7702	–	–	–
Exp/theo. [19]	5.611	12.6885	0.2415	0.0086	0.2126
Theo [32,33]	5.61	12.71	–	–	–
Exp. [77]	5.6034	12.6937	0.2336 (4)	0.0976 (6)	0.0499 (6)

The density of state (DOS) was obtained to analyze the corresponding electronic structures.

Based on the theoretical and experimental results, seven models were constructed using a single conventional $1 \times 1 \times 1$ cell as a repeating unit to represent bulk and surface structures. First, structural and electronic properties were calculated for a perfect bulk $BaWO_4$ lattice (Fig. 1).

The representation of the $BaWO_4$ bulk structure is shown in Fig. 1. The W atoms are coordinated to four O atoms, producing tetrahedral [WO_4] clusters (with 4 vertices, 4 faces, and 6 edges). Correspondingly, the Ba atoms are coordinated to eight O atoms, resulting in a formation of [BaO_8] clusters (with 8 vertices, 12 faces, and 18 edges) [67].

In the second step, different surfaces were modeled by using unreconstructed (truncated bulk) [68] slab models with calculated equilibrium geometries. The (001), (101), (110), (100), (111), and (112) surfaces of $BaWO_4$ were simulated considering symmetrical slabs (with respect to the mirror plane). All surfaces were terminated with O planes; and after the corresponding optimization process and thickness convergence tests, the resulting slab models consisted of four molecular units containing 24 atoms, as shown in Fig. 2.

Note that the (101), (111), and (112) surfaces are terminated with W and O atoms, while the other listed surfaces are Ba–O terminated. The W surface atoms are coordinated to three or four O atoms, forming [WO_3] or [WO_4] clusters, respectively, while the Ba surface atoms are coordinated to three, five, or six O atoms, forming [BaO_3], [BaO_5] or [BaO_6] clusters, respectively.

Present equilibrium morphology models are derived from calculated surface energies [65,69,70] using the assumption that crystal faces with lowest surface energies control the crystal morphology [71–73]. Since surface stability depends on atomic configurations of exposed facets [74], the local coordination of both the W and Ba atoms controls the crystal morphology of $BaWO_4$ and corresponding behavior of each surface (as shown in Fig. 2).

Another important aspect that should be considered when studying solid materials is a distinction between the surface energy, E_{surf}, and the surface tension, σ. The surface tension is a "surface stress" represented by a work force per unit area in the surface layer [75,76]. The surface tension can be obtained using the thermodynamic stability model described by the equation $\sigma = \partial E_{tot}/\partial A$, where E_{tot} is the total energy with contributions from the particle bulk and surfaces. To calculate E_{tot}, uniform dilation with an area, ΔA (corresponding to a constant ratio between the in-plane lattice parameters x:y) of the structure must be performed while optimizing only the internal parameters (without optimization of the in-plane cell parameters). Thus, E_{tot} can be calculated as $\frac{1}{2}(E_{slab} - nE_{bulk})$ for optimized structures and surfaces after dilation. Therefore, by applying two-dimensional dilation to a slab in the surface plane and calculating the total energy as previously described, a change in total energy (ΔE_{tot}) after dilation could be obtained for a given dilation area value.

3. Results and discussion

3.1. X-ray diffraction measurements and Rietveld refinements

The crystal structure, the lattice parameters and the atomic positions were obtained by using the Rietveld refinement method (Fig. 3). The calculated values for the $BaWO_4$ structure are collected in Table 1 and compared with experimental ones, as well as with previous theoretical and experimental results [19,32,33].

The Rietveld refinement results indicate that the obtained diffraction patterns for the $BaWO_4$ crystals match the corresponding spectra in the Inorganic Crystal Structure Database (ICSD, card N° 250487) [77], as shown in Fig. 3, which compares the observed patterns with the calculated ones. Low deviation values for the statistical parameters R_{wp}, R_p, R_{Bragg}, and χ^2 (14.73%, 9.32%, 5.45% and 1.29%, respectively) were found, which indicate good quality of the structural refinements. The lattice parameters (a, b=5.6149 Å, c=12.7326 Å and $\alpha=\beta=\gamma=90°$) estimated from the refinements correspond to a tetragonal structure with space group $I4_1/a$ (N° 88) and four molecular formula units per unit cell (Z=4), which confirms the applicability of the CP method to the synthesis of $BaWO_4$ crystals.

As can be observed in Table 1, the agreement of our calculations with the experiments is reasonably good, being the unit-cell volume underestimated by 3.3% and the axial ratio c/a agrees within 2.2%. In addition, our structural data are according to previously reported theoretical and experimental results.

3.2. Band structure and density of states

The band structures and projected DOS for atoms and orbitals in the bulk $BaWO_4$ and (001), (101), (110), (100), (111), and (112) surfaces are presented in Fig. 4.

The analysis of the principal components of atomic orbitals (AOs) for selected bands shows that the $BaWO_4$ valence band (VB) mostly consists of $2p_x$, $2p_y$, and $2p_z$ orbitals of the O atoms, with the most important contribution coming from the $2p_x$ orbitals. The

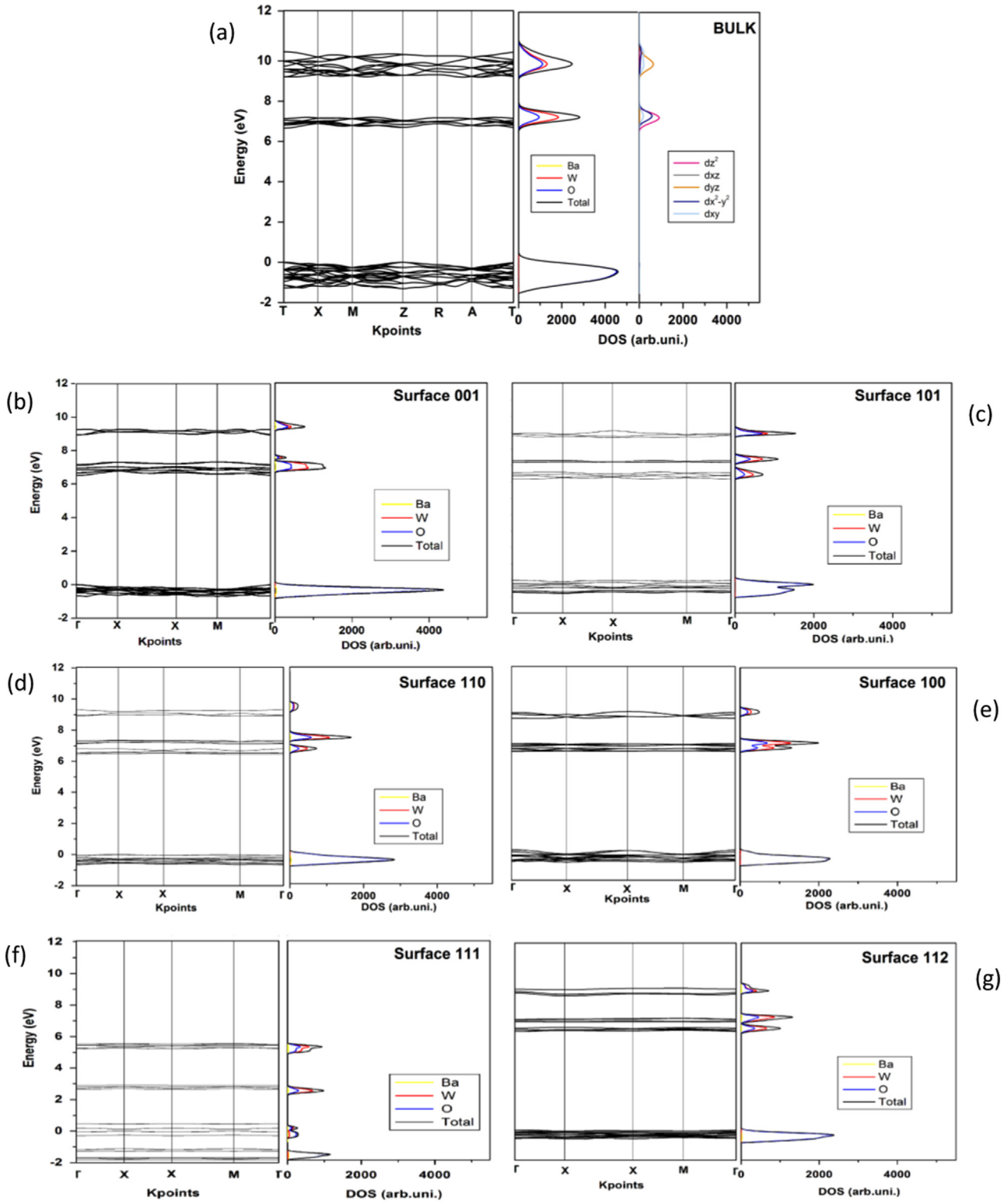

Fig. 4. Calculated band structures and DOS for the (a) bulk $BaWO_4$ and (b) (001), (c) (101), (d) (110), (e) (100), (f) (111), and (g) (112) surfaces.

lowest part of the conduction band (CB) is composed of the $5d_z^2$, $5d_{xz}$, $5d_{yz}$, $5d_{x2-y2}$, and $5d_{xy}$ AOs of the W atoms, with the $5d_z^2$ orbitals being the most important components for the bulk $BaWO_4$.

The band structure and DOS projected for the (001), (101), (110), (100), (111), and (112) surfaces are shown in Fig. 4(b–g). The gap energy, E_{gap}, obtained for these surfaces is very similar to that for the bulk crystal (see Table 2). However, the bands contributing to the lowest part of the CB have different arrangements for each studied surface, which affect the contribution of the W 5d orbitals depending on the selected surface. It should be noted that the (111) surface exhibits conducting behavior.

Table 2
Calculated values of the surface energy, surface tension, gap energy, and change in total energy (ΔE_{tot}) for a given value of dilation area (ΔA) for each surface.

Surface	E_{suf} (J/m^2)	ΔE_{tot} (Hartree)	ΔA (Å^2)	σ (J/m^2)	E_{gap}(eV)
(112)	0.92	0.034	2.350	0.73	6.60
(001)	1.02	0.034	1.263	0.57	6.52
(110)	1.10	0.034	1.982	0.85	6.45
(100)	1.22	0.039	2.803	1.09	6.47
(101)	1.31	0.039	1.537	0.91	6.17
(111)	2.06	0.020	4.161	2.58	Conductor

3.3. FE-SEM analyses and morphologies of the $BaWO_4$ crystals

The morphologies of the $BaWO_4$ crystals obtained by FE–SEM are depicted in Fig. 5.

As shown by the obtained experimental micrographs (Fig. 5) [15], crystal morphologies can be modified by tuning surface energy values for various facets using the Wulff theorem and the related construction method [65]. Taking into account the (001), (101), (110), (100), (111), and (112) facets, various crystal morphologies for $BaWO_4$ are displayed in Fig. 6.

Fig. 2 shows the local coordination (clusters) for both the Ba and W atoms of the (001), (101), (110), (100), (111), and (112) surfaces. One of the most pronounced differences between the bulk and surface structural properties is that due to the reduced coordination of the O atoms in the top layers, the resulting vacancies produce spacing between the adjacent layers, thus providing a change in the values of the surface energy, i.e. modifying the stability of the surfaces to generate the corresponding morphology [78].

This observation can be confirmed by the detailed analysis of the results presented in Fig. 4, indicating small changes in the CB for each studied surface as compared to the bulk. The E_{gap} surface values follow the order of stability for the $BaWO_4$ surfaces obtained from the results of theoretical calculations, which is (112) > (001) > (110) > (100) > (101) > (111). Recent works of Gao et al. [78,79] revealed that the morphology of scheelite crystals present predominantly the exposed (112), (001), and (100) surfaces, being the (112) surface the most stable. This result agrees with our present data and previous results reported in the literature [80,81]. Table 2 lists the corresponding values of the surface energy and tension. The analysis of the obtained results reveals a similar trend for the given values except for the most stable

Fig. 5. FE–SEM images of the $BaWO_4$ crystals.

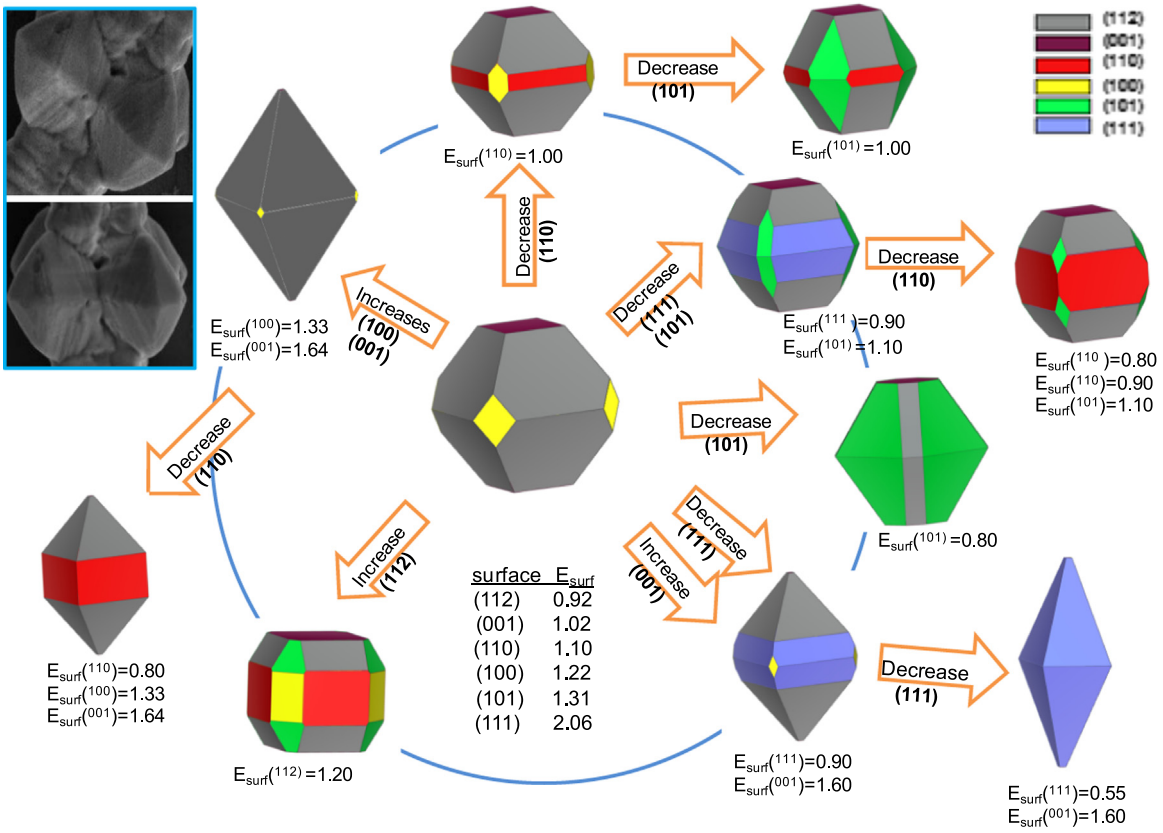

Fig. 6. Crystallographic structures and morphology map for the $BaWO_4$ crystals (the surface energy units are given in J/m^2). The experimental FE–SEM images (inset) are included for comparison.

surface, (112), which exhibits a higher value of surface tension than that for (001). This phenomenon can be explained by noticing that the (112) surface termination contains a large number of undercoordinated atoms (relative to the bulk coordination) with only three O atoms coordinated to each Ba atom. In addition, the (101) surface is characterized by a low value of surface tension, consistent with high stability due to six-coordinated Ba atoms, which is observed only for the (001) and (101) surfaces.

The analysis of the theoretical results indicates that the most stable surfaces are the (112), (001), and (100) facets [−7879], which can form a truncated octahedron corresponding to the ideal morphology (shown in the central part of Fig. 6). When the relative stability of the facets changes (increases or decreases), more than one facet type appears in the resulting morphology, producing morphology variations. A truncated cube can be obtained if the surface energy of (112) is increased to 1.20 J/m^2, while a edge-truncated octahedron can be produced when the surface energy of (101) is decreased to 0.80 J/m^2 (see Fig. 6). Central part of some FE-SEM images (shown in Fig. 5) is included in the left inset of Fig. 6, which is the best well-faceted sighting to compare. A good agreement between the experimental and theoretical morphologies is obtained when the values of surface energy for the (001) and (100) facets increase simultaneously (see Fig. 6). Thus, variations in the ratio between values of surface energy affect the related morphologies and thus can be used to obtain correlations with experimental results.

4. Conclusions

Crystal morphology is an important parameter for obtaining high-quality crystals with excellent properties. $BaWO_4$ crystals have been synthesized as representative members of scheelite-based materials by using the CP method. XRD and Rietveld refinement were utilized to structurally characterize the obtained samples, while FE–SEM was used to investigate the morphologies of the as-synthesized structures. The geometry, electronic properties of the bulk, surface energies, and surface tension of the $BaWO_4$ crystals were evaluated using first-principles quantum mechanical calculations.

As a result of this work, the following conclusions were obtained: i) By using the Wulff's theorem, a simple model was proposed to determine surface energies of $BaWO_4$ crystals at atomic-level resolution. ii) The proposed computational technique was utilized to calculate equilibrium crystal morphologies. Using this model, we were able to evaluate possible morphologies and morphological transformations in $BaWO_4$ by controlling the ratio between surface energy values of each facet. iii) The stability order of the $BaWO_4$ surfaces obtained from the theoretical calculations can be expressed as (112) > (001) > (110) > (100) > (101) > (111). Our work indicates that the morphology of scheelite crystals have (112), (001), and (100) as predominantly exposed surfaces, with the (112) facet being the commonly exposed surface. iv) A truncated octahedron corresponds to the ideal morphology predicted for the $BaWO_4$ crystals by theoretical calculations. However, a truncated cube or edge-truncated octahedron can be obtained due to the destabilization of the (112) surface or stabilization of the (101) surface, respectively. v) The obtained experimental and theoretical morphologies are similar when the values of surface energy for the (001) and (100) facets increase simultaneously.

Modulations of the $BaWO_4$ crystal morphologies resulting from the theoretical simulations have been applied to explain the changes observed at experimental conditions and clarify how the knowledge of surface-specific properties can be utilized to design crystal morphologies that exhibit improved performance in various applications. Using this knowledge, such modeling type can

serve as a predictive tool to modify and ultimately control crystal morphologies. Therefore, computational techniques combined with experimental methods can be utilized to study morphologies of materials that can profoundly affect their physical and chemical properties as well as to improve the related performance of materials and innovate the material design.

Acknowledgments

This work was financially supported by the following Spanish research funding institutions: CTQ2012-36253-C03-02 project (Ministerio de Economia y Competitividad), PrometeoII/2014/022 and ACOMP/2014/270 projects (Generalitat Valenciana), Brazilian Research Funding Institutions: CNPq (INCTMN 573636/2008-7), FAPESP-CDMF (2013/07296-2), CAPES/PNPD 1268069, CAPES (process A104/2013 and 99999.002998/2014-09), and Programa de Cooperación Científica con Iberoamerica (Brasil) of Ministerio de Educación (PHBP14-00020). J.A. acknowledges to Ministerio de Economia y Competitividad, "Salvador Madariaga" program, PRX15/00261. L.G. acknowledges Banco Santander (Becas Iberoamérica: Jóvenes profesores e investigadores). M.C. acknowledges Generalitat Valenciana for Santiago Grisolia Program 2015/033.

References

[1] M. Kobayashi, M. Ishiib, K. Haradab, Y. Uski, H. Okuno, H. Shimizu, T. Yazawab, Scintillation and phosphorescence of $PbWO_4$ crystals, Nucl. Instrum. Methods A 373 (1996) 333–346.
[2] L.S. Cavalcante, J.C. Sczancoski, J.W.M. Espinosa, J.A. Varela, P.S. Pizani, E. Longo, Photoluminescent behavior of $BaWO_4$ powders processed in microwave-hydrotherm, J. Alloy. Compd. 474 (2009) 195–200.
[3] R. Dhilip Kumar, S. Karuppuchamy, Microwave-assisted synthesis of copper tungstate nanopowder for supercapacitor applications, Ceram. Int. 40 (2014) 12397–12402.
[4] J. Zhang, J. Pan, L. Shao, J. Shu, M. Zhou, J. Pan, Micro-sized cadmium tungstate as a high-performance anode material for lithium-ion batteries, J. Alloy. Compd. 614 (2014) 249–252.
[5] C. Anil Kumar, D. Pamu, Dielectric and electrical properties of $BaWO_4$ film capacitors deposited by RF magnetron sputtering, Ceram. Int. 41 (2015) S296–S302.
[6] C. Shivakumara, R. Saraf, S. Behera, N. Dhananjaya, H. Nagabhushana, Scheelite-type MWO_4 (M=Ca, Sr, and Ba) nanophosphors: facile synthesis, structural characterization, photoluminescence, and photocatalytic properties, Mater. Res. Bull. 61 (2015) 422–432.
[7] F.M. Pontes, M.A.M.A. Maurera, A.G. Souza, E. Longo, E.R. Leite, R. Magnani, M. A.C. Machado, P.S. Pizani, J.A. Varela, Preparation, structural and optical characterization of $BaWO_4$ and $PbWO_4$ thin films prepared by a chemical route, J. Eur. Ceram. Soc. 2 (2003) 3001–3007.
[8] D. Rangappa, T. Fujiwara, M. Yoshimura, Synthesis of highly crystallized $BaWO_4$ film by chemical reaction method at room temperature, Solid State Sci. 8 (2006) 1074–1078.
[9] M.A.P. Almeida, L.S. Cavalcante, M. Siu Li, J.A. Varela, E. Longo, Structural refinement and photoluminescence properties of $MnWO_4$ nanorods obtained by microwave-hydrothermal synthesis, J. Inorg. Organomet. Polym. Mater. 22 (2011) 264–271.
[10] Y. Shen, W. Li, T. Li, Microwave-assisted synthesis of $BaWO_4$ nanoparticles and its photoluminescence properties, Mater. Lett. 65 (2011) 2956–2958.
[11] P.F.S. Pereira, I.C. Nogueira, E. Longo, E.J. Nassar, I.L.V. Rosa, L.S. Cavalcante, Rietveld refinement and optical properties of $SrWO_4$: Eu^{3+} powders prepared by the non-hydrolytic sol–gel method, J. Rare Earth 33 (2015) 113–128.
[12] I.M. Pinatti, I.C. Nogueira, W.S. Pereira, P.F. Pereira, R.F. Goncalves, J.A. Varela, E. Longo, I.L. Rosa, Structural and photoluminescence properties of $Eu^{(3+)}$ doped alpha-Ag_2WO_4 synthesized by the green coprecipitation methodology, Dalton Trans. 44 (2015) 17673–17685.
[13] J.C. Rendón-Angeles, Z. Matamoros-Veloza, J. López-Cuevas, I.A. Gonzalez, K. L. Montoya-Cisneros, K. Yanagisawa, J. Willis-Richards, J. Diaz-Algara, Rapid synthesis of scheelite $SrWO_4$ particles using a natural $SrSO_4$ ore under alkaline hydrothermal conditions, Hydrometallurgy 157 (2015) 116–126.
[14] A. Phuruangrat, T. Thongtem, S. Thongtem, Precipitate synthesis of $BaMoO_4$ and $BaWO_4$ nanoparticles at room temperature and their photoluminescence properties, Superlattice Microstruct. 52 (2012) 78–83.
[15] M. Li, Y. Guan, Y. Yin, X. Cui, S. Rong, G. Jin, Y. Hao, Q. Wu, Controllable synthesis of 3D $BaXO_4$ (X=W, Mo) microstructures by adjusting nucleation stage and their photoluminescence properties, Superlattice Microstruct. 80 (2015) 222–228.
[16] F.J. Manjón, D. Errandonea, N. Garro, J. Pellicer-Porres, P. Rodríguez-Hernández, S. Radescu, J. López-Solano, A. Mujica, A. Muñoz, Lattice dynamics study of scheelite tungstates under high pressure I. $BaWO_4$, Phys. Rev. B 74 (2006) 144111.
[17] B. Sun, Y. Liu, W. Zhao, J. Wu, P. Chen, Hydrothermal preparation and white-light-controlled resistive switching behavior of $BaWO_4$ nanospheres, Nano-Micro Lett. 7 (2015) 80–85.
[18] L.S. Cavalcante, F.M.C. Batista, M.A.P. Almeida, A.C. Rabelo, I.C. Nogueira, N. C. Batista, J.A. Varela, M.R.M.C. Santos, E. Longo, M. Siu Li, Structural refinement, growth process, photoluminescence and photocatalytic properties of $(Ba_{1-x}Pr_{2x/3})WO_4$ crystals synthesized by the coprecipitation method, RSC Adv. 2 (2012) 6438–6454.
[19] M. Tyagi, S.G. Singh, A.K. Chauhan, S.C. Gadkari, First principles calculation of optical properties of $BaWO_4$: a study by full potential method, Phys. B 405 (2010) 4530–4535.
[20] D. Ran, H. Xia, S. Sun, P. Zhao, F. Liu, Z. Ling, W. Ge, H. Zhang, J. Wang, Optical phonon modes and transmissivity in $BaWO_4$ single crystal, Cryst. Res. Technol. 41 (2006) 1189–1193.
[21] C. Kavitha, C. Narayana, B.E. Ramachandran, N. Garg, S.M. Sharma, Acoustic phonon behavior of $PbWO_4$ and $BaWO_4$ probed by low temperature Brillouin spectroscopy, Solid State Commun. 202 (2015) 78–84.
[22] H.W. Eng, P.W. Barnes, B.M. Auer, P.M. Woodward, Investigations of the electronic structure of d^0 transition metal oxides belonging to the perovskite family, J. Solid State Chem. 175 (2003) 94–109.
[23] P. Parhi, T.N. Karthik, V. Manivannan, Synthesis and characterization of metal tungstates by novel solid-state metathetic approach, J. Alloy. Compd. 465 (2008) 380–386.
[24] Y. Mi, Z. Huang, F. Hu, X. Li, Room temperature reverse-microemulsion synthesis and photoluminescence properties of uniform $BaMoO_4$ submicro-octahedra, Mater. Lett. 63 (2009) 742–744.
[25] Z. Luo, H. Li, J. Xia, W. Zhu, J. Guo, B. Zhang, Controlled synthesis of different morphologies of $BaWO_4$ crystals via a surfactant-assisted method, J. Cryst. Growth 300 (2007) 523–529.
[26] X. Wu, J. Du, H. Li, M. Zhang, B. Xi, H. Fan, Y. Zhu, Y. Qian, Aqueous mineralization process to synthesize uniform shuttle-like $BaMoO_4$ microcrystals at room temperature, J. Solid State Chem. 180 (2007) 3288–3295.
[27] J.C. Sczancoski, L.S. Cavalcante, N.L. Marana, R.O.D. Silva, R.L. Tranquilin, M. R. Joya, P.S. Pizani, J.A. Varela, J.R. Sambrano, M.S. Li, E. Longo, J. Andrés, Electronic structure and optical properties of $BaMoO_4$ powders, Curr. Appl. Phys. 10 (2010) 614–624.
[28] J.H. Ryu, J.W. Yoon, K.B. Shim, Microwave-assisted synthesis of $BaMoO_4$ nanocrystallites by a citrate complex method and their anisotropic aggregation, J. Alloy. Compd. 413 (2006) 144–149.
[29] A. Phuruangrat, T. Thongtem, S. Thongtem, Barium molybdate and barium tungstate nanocrystals synthesized by a cyclic microwave irradiation, J. Phys. Chem. Solids 70 (2009) 955–959.
[30] M. Anicete-Santos, F.C. Picon, C. Nahum Alves, P.S. Pizani, J.A. Varela, E. Longo, The role of short-range disorder in $BaWO_4$ crystals in the intense green photoluminescence, J. Phys. Chem. C 115 (2011) 12180–12186.
[31] O. Gomis, J.A. Sanz, R. Lacomba-Perales, D. Errandonea, Y. Meng, J.C. Chervin, A. Polian, Complex high-pressure polymorphism of barium tungstate, Phys. Rev. B 86 (2012) 054121.
[32] H. Zhang, T. Liu, Q. Zhang, Xi'en Wang, J. Yin, M. Song, X. Guo, First-principles study on electronic structures of $BaWO_4$ crystals containing F-type color centers, J. Phys. Chem. Solids 69 (2008) 1815–1819.
[33] H. Zhang, T. Liu, Q. Zhang, Xi'en Wang, X. Guo, M. Song, J. Yin, First-principles study on electronic structures and absorption spectra for $BaWO_4$ crystal containing barium vacancy, Nucl. Instrum. Methods B 267 (2009) 1056–1060.
[34] G. Dhanaraj, K. Byrappa, V. Prasad, M. Dudley, Provides the Reader with the Most Complete State-of-the-Art Presentation on the Basics and Realization of Crystal Growth, Springer Handbook of Crystal Growth, Springer-Verlag Berlin Heidelberg, 2010, ISBN: 978-3-540-74761-1.
[35] Q. Kuang, X. Wang, Z. Jiang, Z. Xie, L. Zheng, High-energy-surface engineered metal oxide micro- and nanocrystallites and their applications, Acc. Chem. Res. 47 (2014) 308–318.
[36] K. Huang, L. Yuan, S. Feng, Crystal facet tailoring arts in perovskite oxides, Inorg. Chem. Front. 2 (2015) 965–981.
[37] G. Zhou, M. Lü, F. Gu, S. Wang, Z. Xiu, Morphology-controlled synthesis of $BaWO_4$ nanocrystals via a surfactant-assisted method, Mater. Lett. 59 (2005) 2706–2709.
[38] L.S. Cavalcante, J.C. Sczancoski, L.F. Lima Jr., J.W.M. Espinosa, P.S. Pizani, J. A. Varela, E. Longo, Synthesis, characterization, anisotropic growth and photoluminescence of $BaWO_4$, Cryst. Growth Des. 9 (2009) 1002–1012.
[39] Y. Yin, F. Yang, Y. Yang, Z. Gan, Z. Qin, S. Gao, B. Zhou, X. Li, Controlled synthesis of $BaWO_4$ hierarchical nanostructures by exploiting oriented attachment in the solution of H_2O and C_2H_5OH, Superlattice Microstruct. 49 (2011) 599–607.
[40] C. Cui, J. Bi, D. Gao, K. Zhao, Morphology and crystal phase control in preparation of highly crystallized $BaWO_4$ film via galvanic cell method, J. Alloy. Compd. 462 (2008) L16–L19.
[41] D.G. Stroppa, L.A. Montoro, A. Campello, L. Gracia, A. Beltrán, J. Andrés, E. R. Leite, A.J. Ramirez, Prediction of dopant atom distribution on nanocrystals using thermodynamic arguments, Phys. Chem. Chem. Phys. 16 (2014) 1089–1094.
[42] M.R.D. Bomio, R.L. Tranquilin, F.V. Motta, C.A. Paskocimas, R.M. Nascimento, L. Gracia, J. Andres, E. Longo, Toward understanding the photocatalytic activity of $PbMoO_4$ powders with predominant (111), (100), (011), and (110) facets. A

combined experimental and theoretical study, J. Phys. Chem. C 117 (2013) 21382–21385.
[43] V.M. Longo, L. Gracia, D.G. Stroppa, L.S. Cavalcante, M. Orlandi, A.J. Ramirez, E. R. Leite, J. Andrés, A. Beltrán, J.A. Varela, E. Longo, A joint experimental and theoretical study on the nanomorphology of $CaWO_4$ crystals, J. Phys. Chem. C 115 (2011) (2011) 3–20119.
[44] J. Andrés, L. Gracia, L., A.F. Gouveia, M.M. Ferrer, E. Longo, Effects of surface stability on the morphological transformation of metals and metal oxides as investigated by first principles calculations, Nanotechnology 26 (2015) 405703.
[45] M.M. Ferrer, A.F. Gouveia, L. Gracia, E. Longo, J. Andrés, A 3D platform for the morphology modulation of materials: first principles calculations on the thermodynamic stability and surface structure of metal oxides: Co_3O_4, α-Fe_2O_3, and In_2O_3, Model. Simul. Mater. Sci. Eng. 24 (2016) 025007.
[46] R.A. Roca, J.C. Sczancoski, I.C. Nogueira, M.T. Fabbro, H.C. Alves, L. Gracia, L.P. S. Santos, C.P. de Sousa, J. Andrés, G.E. Luz, E. Longo, L.S. Cavalcante, Facet-dependent photocatalytic and antibacterial properties of α-Ag_2WO_4 crystals: combining experimental data and theoretical insights, Catal. Sci. Technol. 5 (2015) 4091–4107.
[47] G. Botelho, J. Andres, L. Gracia, L.S. Matos, E. Longo, Photoluminescence and photocatalytic properties of Ag_3PO_4 microcrystals: an experimental and theoretical investigation, ChemPlusChem 81 (2016) 202–212.
[48] M.T. Fabbro, C. Saliby, L.R. Rios, F.A. La Porta, L. Gracia, M.S. Li, J. Andrés, L.P. S. Santos, E. Longo, Identifying and rationalizing the morphological, structural, and optical properties of β-Ag_2MoO_4 microcrystals, and the formation process of Ag nanoparticles on their surfaces: combining experimental data and first-principles calculations, Sci. Technol. Adv. Mater. 16 (2015) 065002.
[49] H.M. Rietveld, A profile refinement method for nuclear and magnetic structures, J. Appl. Cryst. 2 (1969) 65–71.
[50] A.C. Larson, R.B.V. Dreele, General Structure Analysis System (GSAS), Los Alamos National Laboratory, New Mexico, USA, 2004, Report LAUR.
[51] L.W. Finger, D.E. Cox, A.P. Jephcoat, A correction for power diffraction peak asymmetry due to axial divergence, J. Appl. Cryst. 27 (1994) 892–900.
[52] P.W. Stephens, Phenomenological model of anisotropic peak broadening in power diffraction, J. Appl. Cryst. 32 (1999) 281–289.
[53] R. Dovesi, V.R.S., C. Roetti, R. Orlando, C.M. Zicovich-Wilson, F. Pascale, B. Civalleri, K. Doll, N.M. Harrison, I.J. Bush, P.H. D'Arco, M. Llunell, M. Causa, Y. Noël, CRYSTAL14 User's Manual, University of Torino, Torino, 2014.
[54] A.D. Becke, Perspective on density functional thermochemistry. III. The role of exact exchange, J. Chem. Phys. 98 (1993) 5648–5652.
[55] C.T. Lee, W.T. Yang, R.G. Parr, Development of the Colle–Salvetti correlation-energy formula into a functional of the electron density, Phys. Rev. B: Condens. Matter 37 (1988) 785–789.
[56] M.L. Moreira, J. Andres, L. Gracia, A. Beltrán, L.A. Montoro, J.A. Varela, E. Longo, Quantum mechanical modeling of excited electronic states and their relationship to cathodoluminescence of $BaZrO_3$, J. Appl. Phys. 114 (2013) 043714.
[57] L. Gracia, V.M. Longo, L.S. Cavalcante, A. Beltran, W. Avansi, M.S. Li, V. R. Mastelaro, J.A. Varela, E. Longo, J. Andres, Presence of excited electronic state in $CaWO_4$ crystals provoked by a tetrahedral distortion: an experimental and theoretical investigation, J. Appl. Phys. 110 (2011) 043501.
[58] E. Longo, D.P. Volanti, V.M. Longo, L. Gracia, I.C. Nogueira, M.A.P. Almeida, A. N. Pinheiro, M.M. Ferrer, L.S. Cavalcante, J. Andrés, Toward an understanding of the growth of Ag filaments on α-Ag_2WO_4 and their photoluminescent properties: a combined experimental and theoretical study, J. Phys. Chem. C 118 (2014) 1229–1239.
[59] F.M.C. Batista, F.A. La Porta, L. Gracia, E. Cerdeiras, L. Mestres, M. Siu Li, N. C. Batista, J. Andrés, E. Longo, L.S. Cavalcante, A joint experimental and theoretical study on the electronic structure and photoluminescence properties of $Al_2(WO_4)_3$ powders, J. Mol. Struct. 1081 (2015) 381–388.
[60] A. Beltrán, L. Gracia, E. Longo, J. Andrés, First-principles study of pressure-induced phase transitions and electronic properties of Ag_2MoO_4, J. Phys. Chem. C 118 (2014) 3724–3732.
[61] H.J. Monkhorst, J.D. Pack,, Special points for Brillouin-x. One integrations, Phys. Rev. B: Condens. Matter 13 (1976) 5188–5192.
[62] F. Cora, A. Patel, N.M. Harrison, R. Dovesi, C.R.A. Catlow, An ab initio Hartree–Fock study of the cubic and tetragonal phases of bulk tungsten trioxide, J. Am. Chem. Soc. 118 (1996) 12174–12182.
[63] CRYSTAL Basis set. ⟨http://www.crystal.unito.it/Basis_Sets/Ptable.html⟩, 2016 (accessed 10.02.16).
[64] Basis set. ⟨http://www.tcm.phy.cam.ac.uk/~mdt26/basis_sets/Ba_basis.txt⟩, 2016 (accessed 10.02.16).
[65] G. Wulff, Zur Frage der Geschwindigkeit Des Wachstums und Der Auflosung der Krystallflachen, Krist. Miner. 34 (1901) 449–530.
[66] K. Momma, F. Izumi, VESTA 3 for three-dimensional visualization of crystal, volumetric and morphology data, J. Appl. Cryst. 44 (2011) 1272–1276.
[67] A. Kuzmin, J. Purans, Local atomic and electronic structure of tungsten ions in AWO_4 crystals of scheelite and wolframite types, Radiat. Meas. 33 (2001) 583–586.
[68] F. Toa, Z. Wang, L. Yao, W. Cai, X. Li, Shape-controlled synthesis and characterization of YF_3 truncated octahedral nanocrystals, Cryst. Growth Des. 7 (2007) 854–858.
[69] C. Herring, Some theorems on the free energies of crystal surfaces, Phys. Rev. 82 (1981) 87–93.
[70] J.W. Gibbs, A.W. Smith, On the equilibrium of heterogeneous substances, Trans. Conn. Acad. Arts Sci. 3 (1875) 108–248.
[71] X. Wang, H. Xu, H. Wang, H. Yan, Morphology-controlled $BaWO_4$ powders via a template-free precipitation technique, J. Cryst. Growth 284 (2005) 254–261.
[72] Y. Liu, Y. Chu, Surfactant-assisted synthesis of single crystal $BaWO_4$ octahedral microparticles, Mater. Chem. Phys. 92 (2005) 59–63.
[73] B. Xie, Y. Wu, Y. Jiang, F. Li, J. Wu, S. Yuan, W. Yu, Y. Qian, Shape-controlled synthesis of $BaWO_4$ crystals under different surfactants, J. Cryst. Growth 235 (2002) 283–286.
[74] L.D. Marks, Modified wulff constructions for twinned particles, J. Cryst. Growth 61 (1983) 556–566.
[75] A.S. Barnard, P. Zapol, Effects of particle morphology and surface hydrogenation on the phase stability of TiO_2, Phys. Rev. B 70 (2004) 235403.
[76] L. Li, F. Abild-Pedersen, J. Greeley, J.K. Nørskov, Surface tension effects on the reactivity of metal nanoparticles, J. Phys. Chem. Lett. 6 (2015) 3797–3801.
[77] D. Errandonea, J. Pellicer-Porres, F.J. Manjón, A. Segura, Ch Ferrer-Roca, R. S. Kumar, O. Tschauner, J. López-Solano, P. Rodríguez-Hernández, S. Radescu, A. Mujica, A. Muñoz, G. Aquilanti, Determination of the high-pressure crystal structure of $BaWO_4$ and $PbWO_4$, Phys. Rev. B 73 (2006) 224103.
[78] Y. Hu, Z. Gao, W. Sun, X. Liu, Anisotropic surface energies and adsorption behaviors of scheelite crystal, Colloids Surf. A 415 (2012) 439–448.
[79] Z.Y. Gao, W. Sun, Y.H. Hu, X.-W. Liu, Surface energies and appearances of commonly exposed surfaces of scheelite crystal, Trans. Nonferr. Met. Soc. 23 (2013) 2147–2152.
[80] T.G. Cooper, N.H. de Leeuw, A combined ab initio and atomistic simulation study of the surface and interfacial structures and energies of hydrated scheelite: introducing a $CaWO_4$ potential model, Surf. Sci. 531 (2003) 159–176.
[81] H.-Y. Jung, Y.-D. Huh, A two-dimensional four-fold symmetric $SrMoO_4$ dendrite, CrystEngComm 17 (2015) 1398.